nature geoscience

SUPPLEMENTARY INFORMATION

DOI: 10.1038/NGEO1273

Eddy-induced reduction of biological production in eastern boundary upwelling systems

Nicolas Gruber[1], Zouhair Lachkar[1], Hartmut Frenzel[2], Patrick Marchesiello[3], Matthias Münnich[1], James C. McWilliams[2,*], Takeyoshi Nagai[4] & Gian-Kasper Plattner[1,‡]

[1]*Environmental Physics, Institute of Biogeochemistry and Pollutant Dynamics, ETH Zurich, Zurich, Switzerland.*

[2]*Department of Atmospheric and Oceanic Sciences, UCLA, Los Angeles, CA, USA.*

[3]*Institut de Recherche pour le Développement, LEGOS, 31400 Toulouse, France.*

[4]*Tokyo University of Marine Science and Technology, Tokyo, Japan.*

**also at Institute of Geophysics and Planetary Physics, UCLA, Los Angeles, CA, USA.*

‡now at Climate and Environmental Physics, University of Bern, Bern, Switzerland.

Nature Geoscience, August 20, 2011

The supplementary material contains four sections. In the first section, additional plots and results are presented and discussed to support the finding from our comparative study of the four major eastern boundary upwelling systems that higher levels of eddy-kinetic energy are associated with lower levels of primary production. The standard (eddying) model is evaluated against observations in the second section. In the third section, results are described from additional simulations that are used to assess the impact of eddies, in particular simulations with different resolutions and topographies to induce different levels of eddy-kinetic

energy. The forth and final section describes the Reynolds decomposition method used to diagnose the eddy-driven total nitrogen fluxes.

1 Comparison between the eastern boundary current systems

Details of the data sources and methods are given in the method section of the main text.

Figures S.1-S.3 reveal the large differences in annual mean NPP, upwelling strength, and eddy-kinetic energy between the four major eastern boundary upwelling systems considered here, i.e., California Current System (CalCS), Canary Current System (CanCS), Humboldt Current System (HumCS), and Benguela Current System (BenCS). The 2° binned and averaged data are then displayed in Figure S.4. They were then binned further to 4°bins for the correlation and multiple linear regression analyses.

Table S.1 lists the results of the multiple linear regression analyses and the associated linear correlation coefficients for the 4°bin averages (r^2). Also listed are the coefficients associated with each independent variable. The projected results of our standard multiple linear regression, i.e., that with upwelling strength and eddy-kinetic energy as independent variables, are then displayed in Figure 1 in the main text. All regressions yield for NPP versus EKE a negative slope with values between -0.22 and -0.39 mol C m^{-2} yr^{-1} cm^{-2} s^2. This slope is substantially larger than that found by our model simulations (see below). We interpret this large difference to be a consequence of two re-inforcing biases: On the one hand, our model tends to underpredict NPP (see next section). Assuming that this underprediction is proportional to the magnitude of NPP,

we would then underpredict the slope of NPP versus EKE. On the other hand, comparisons of the standard VGPM parameterization for NPP with in-situ data in the CalCS revealed a tendency for over-estimation in near-shore areas [1]. This bias in the observationally based estimates of NPP toward high values likely causes a slope that is too steep. We did not make an attempt to correct for this bias in the observationally based estimates of NPP, as it is not clear whether the retuned parameters for the CalCS are valid in the other EBUS as well.

2 Model evaluation

The employed model is similar to the one described and evaluated earlier [2], but differs in three respects: First, this model is run at a higher resolution. This model has a uniform 5 km resolution throughout the California Current System, while the previous one had a 15 km resolution for the entire system, and employed a 5 km child grid for the central CalCS. Second, the model is based on a newer numerical core, optimized for distributed memory machines. It also contains a few additional modifications, such as an improved implementation of the KPP scheme [3], a stiffer scheme for the vertical sigma coordinate system, resulting in a faster flattening of the sigma layers away from topography, and improved numerics for tracer transport (A. Shchepetkin, pers. comm., 2008). Finally, two parameters of the ecosystem model, i.e., the initial slope of the photosynthesis to light relationship, α_P, and the linear mortality rate of phytoplankton, η_P^{mort}, were modified in order to enhance the model's primary production without altering the relatively good agreement of the model's surface biomass (see below). In particular, α_P was doubled from its original value of 1.0 to 2.0 mg C (mg Chl-a W m^{-2} day)$^{-1}$, and η_P^{mort} was doubled from 0.024 to 0.048 day^{-1}.

These new parameter values are well within the range of values used in other models.

These changes are substantial enough to require a re-evaluation of the model's performance. We use the same satellite-based constraints used in our previous study [2], i.e., primarily satellite chlorophyll and sea-surface temperature (SST), and augmented them with a satellite-based estimate of NPP on the basis of the Vertically Generalized Production Model [4], with the parameters tuned to fit a large set of in-situ observations from the CalCOFI program (see [1] for details). We also include again observations from CalCOFI line 70, which starts in Monterey Bay (37°N, 121.8°W) and extends several hundred kilometers into the open ocean to 32°N, 135°W. For all evaluations, only the simulation with eddies is considered. In fact, the non-eddy simulation compares considerably worse against observations than the standard (eddying) simulation. This is, of course, as expected since the non-eddy simulation was intended as an extreme case to explore the sensitivity of the system to changes in circulation.

The comparison of the modeled annual mean chlorophyll in the near-surface with that inferred by SeaWiFS (Figure S.5a, b) demonstrates the ability of the model to capture the time-mean large-scale distribution of chlorophyll in the CalCS. In comparison with the 15+5 km version [2], this version has slightly higher near-surface chlorophyll levels throughout much of the central CalCS, extending further into the offshore region.

A more quantitative comparison between the modeled and observed chlorophyll distributions is depicted in the Taylor diagrams shown in Figure S.6 [5]. A Taylor diagram combines information about the correlation between the modeled and observed pattern (plotted as the angle between the

abscissa and the line drawn from the origin to the point) with the standard deviation of the modeled field relative to that of the observed field (distance from origin to the point along the angle given by the correlation). On this plot, the observed pattern lies on the abscissa at distance 1 from the origin, since it correlates perfectly with itself and has a normalized standard deviation of 1. The centered pattern root mean square (RMS) error is then given by the distance between the point defined by the modeled pattern and the observed pattern. The shorter this distance, the greater the agreement between the pattern.

Figure S.6a shows for the annual mean chlorophyll pattern over the entire domain (point denoted by "DOMAIN") a correlation of 0.8, substantially better than was achieved by the previous 15+5 km model (less than 0.6). Every sub-region within the model's domain has a better agreement with the SeaWiFS observations than was achieved with the previous model. A small downside is that this version tends to have a slightly smaller overall standard deviation, leading to a slightly larger underestimation of the spatial variability compared to SeaWIFS. On the seasonal time-scale, the improvement is not as large, with a few sub-domains having a (slightly) worse agreement with the observations (Figure S.6b).

Similar agreements and disagreements between the model simulated results and the observationally based estimates as found for chlorophyll can be identified for NPP (Figure S.5b, c), although with an overall tendency for the model to be biased low (on average, by about 30% (see Table S.3). The largest underestimation occurs in the nearshore areas, yielding also the lowest overall correlation (Figure S.6c). On average, annual mean NPP compares less favorably to the

observationally based estimate than chlorophyll. However, the achieved correlation coefficient of about 0.8 and the overall skill of the our model with respect to the observations compares very well to what is typically achieved with predictive models and even with different observationally based models of NPP (see e.g., Friedrichs et al. [6]). As was the case for the seasonal component of chlorophyll, the seasonal component of NPP is less well captured by our model (Figure S.6d). Interestingly, the seasonal component of NPP compares better to observations than the seasonal component of chlorophyll. The reason for this apparent inconsistency is that chlorophyll is evaluated only in the near surface, whereas NPP reflects production integrated over the whole water column. The better agreement for the seasonal component of NPP versus the seasonal component of chlorophyll is therefore likely due to the model being able to better capture the seasonal dynamics of production at depth compared to that at the surface. For sea-surface temperature (SST), the 5 km version matches the already excellent agreement of the 15+5 km model with the AVHRR SST observations (Figure S.6e and f).

A comparison of the modeled versus observed vertical distributions of temperature and salinity along CalCOFI line 70 indicates that the simulated vertical gradients are captured well, but that the onshore slope is underestimated, particularly in the nearshore region (Figure S.7a-d). This bias existed already in the 15+5 km simulations (cf. [2]) and was interpreted to be primarily due to our using of COADS winds at that time, which have a too small positive wind stress curl, and thereby cause insufficient lifting of the thermocline. Here, we are using QuikSCAT winds, which exhibit a stronger curl, indicating that other factors, such as e.g., intermittency, must play a role in this underestimation. The model simulates the observed nitrate concentration also reasonably

well (Figure S.7e-f), but suffers from the same bias as temperature and salinity, i.e., the modeled isolines fail to show the shoreward shoaling seen in the observations, particularly in the nearshore region.

In summary, the evaluation of our simulated fields with remotely sensed chlorophyll, NPP, and SST as well as in-situ observations of temperature, salinity, chlorophyll, and nitrate suggest that the model captures the large-scale pattern and their seasonal evolution with similar or even slightly better skill than our previous 15 km + 5 km simulation [2].

3 Investigating the effect of eddies by altering the resolution

To investigate the impact of different levels of eddy-kinetic energy (EKE) on NPP, we used two additional setups, one at 15 km resolution that has a level of EKE that is about 40% lower, and one at 60 km resolution, with a level of EKE that is more than 4-times lower than the standard 5 km setup (see Table S.2). The level of EKE in the model also depends on the bathymetry and coastline [7]. We therefore also consider cases for the 5 km and 15 km setups that employ the bathymetry and coastline of the 60 km model. These latter modifications lead to only minor changes in EKE, however. A summary of the model setups considered is given in Table S.2.

The results from these models confirm the trend established from the difference between the eddy and non-eddy simulations, i.e., that the higher EKE is, the lower are net primary production and export production (Figure S.8). The 60 km model setup corresponds rather closely to the 5 km model without the non-linear terms in the momentum equations, while the 15 km model setup lies

very close to the trend line established by the end-members. A linear regression yields for NPP a slope of -0.048 mol m^{-2} yr^{-1} cm^{-2} s^2 and for EP a slope of -0.011 mol m^{-2} yr^{-1} cm^{-2} s^2 with excellent goodness of fit. Given the negative bias in our model simulated NPP, these slope estimates are likely too small, but clearly support the substantial modifying effect of production by eddies.

In order to test the robustness of our conclusions drawn from the CalCS, we undertook a similar suite of simulations using corresponding setups for the Canary Current System (CanCS)[8]. Our Canary domain extends in latitude from 10°N (latitude of the North Equatorial Current) to 43°N (north-west Iberia) and extends to between 1500 to 2500 km in offshore direction. In order to achieve maximum consistency, the boundary conditions were prepared in an analogous manner as those for the CalCS, and exactly the same set of parameters were used. The modeled chlorophyll of the CanCS model at 5 km compares about equally well to the SeaWiFS based observations as the corresponding model for the CalCS, i.e., the CanCS has a correlation coefficient of about 0.8 and a ratio of the standard deviations of about 0.5, resulting in an overall skill that is nearly identical to the CalCS setup [8]. The results from a suite of CanCS simulations with 5 km, 15 km and 60 km resolution fall nearly on top of those from the CalCS, strongly supporting our conclusions. The results from the 60 km setup of the CalCS may even suggest a steeper slope with regard to NPP.

The spatial distribution of NPP in the 60 km model setup also strongly corresponds to the results of the non-eddying 5 km model (Figure S.10), suggesting that the removal of the non-linear terms in the momentum equations is a robust method to investigate the role of eddies in shaping

the mean state of a system. Also, the alteration of the distribution of nitrate and other tracers (not shown) are rather similar between the 60 km and the non-eddying 5 km models, indicating that the same mechanisms are at work.

In summary, our investigations using a suite of models at varying resolutions and different bathymetries and coastlines fully confirm our findings from the 5 km studies using modifications of the momentum equations. From a model perspective, our findings can be considered as robust.

4 Reynolds decomposition

To decompose the total offshore flux of total organic and total inorganic nitrogen into a mean circulation-driven and into a eddy-driven part, we first computed the time-mean velocity and concentration at each grid-point from the average over 5 years. The temporal deviations of concentrations, velocity, and fluxes were then computed from 2-day averaged outputs corrected for the time-mean part. The use of a mean over several years aliases seasonal variations into the eddy contribution, but this contribution turns out to be rather small (see also [7]). We then averaged the fluxes in the alongshore direction following streamlines. This was done in order to avoid the contribution of permanent meanders, i.e., standing eddies, which substantially contribute to the offshore fluxes as well [9]. By definition, the effects of standing eddies vanish when averaging is along streamlines [10,11]. The streamlines were computed from the geostrophic streamfunction following Karsten and Marshall [11]. To avoid closed contours, we applied a small amount of smoothing before calculating the contours and interpolated linearly between the streamlines and the coastline in the nearshore

100km from the coast.

References

1. Kahru, M., Kudela, R., Manzano-Sarabia, M. & Mitchell, B. G. Trends in primary production in the California Current detected with satellite data. *J. Geophys. Res.* **114** (2009).

2. Gruber, N. *et al.* Eddy-resolving simulation of plankton ecosystem dynamics in the California Current System. *Deep Sea Res. I* **53**, 1483–1516 (2006).

3. Large, W. G., McWilliams, J. C. & Doney, S. C. Oceanic vertical mixing: A review and a model with a nonlocal boundary layer parameterization. *Rev. Geophys.* **32**, 363–403 (1994).

4. Behrenfeld, M. J. & Falkowski, P. G. Photosynthetic rates derived from satellite-based chlorophyll concentration. *Limnol. Oceanogr.* **42**, 1–20 (1997).

5. Taylor, K. E. Summarizing multiple aspects of model performance in a single diagram. *J. Geophys. Res.* **106**, 7183–7192 (2001).

6. Friedrichs, M. A. M. *et al.* Assessing the uncertainties of model estimates of primary productivity in the tropical Pacific Ocean. *Journal of Marine Systems* **76** (2009).

7. Marchesiello, P., McWilliams, J. C. & Shchepetkin, A. F. Equilibrium structure and dynamics of the California Current System. *J. Phys. Oceanogr.* **33**, 753–783 (2003).

8. Lachkar, Z. & Gruber, N. What controls biological productivity in coastal upwelling systems? insights from a comparative modeling study. *Biogeosciences Discuss.* 5617–5652 (2011).

9. Hallberg, R. W. & Gnanadesikan, A. An exploration of the role of transient eddies in determining the transport of a zonally reentrant current. *J. Phys. Oceanogr.* **31**, 3312–3330 (2001).

10. Marshall, J., Olbers, D., Ross, H. & Wolf-Gladrow, D. Potential vorticity constraints on the dynamics and hydrography of the Southern Ocean. *J. Phys. Oceanogr.* **23**, 465–487 (1993).

11. Karsten, R. H. & Marshall, J. Constructing the residual circulation of the ACC from observations. *J. Phys. Oceanogr.* **32**, 33153327 (2002).

Table 1: Results of multiple linear regression analyses for net primary production.[a]

Independent variables[b]	Coefficients[c]	Goodness of fit (r^2)
Net primary production (annual mean) (mol C m^{-2} yr^{-1})		
UWS	a_0 = -2, a_{UWS} = 0.75	0.56
EKE	a_0 = 87, a_{EKE} = -0.39	0.07
UWS, EKE	a_0 = 20, a_{UWS} = 0.75, a_{EKE} = -0.38	0.62
Net primary production (seasonal mean) (mol C m^{-2} yr^{-1})		
UWS	a_0 = 1, a_{UWS} = 0.71	0.49
UWS, EKE	a_0 = 17, a_{UWS} = 0.69, a_{EKE} = -0.22	0.51

[a]: Data were binned to 4° in meridional direction and averaged over a 500 km wide coastal strip, with the exception of EKE, for which only the region from 150 km offshore to 500 km was averaged (see Figure S.1 for boundaries).

[b]: UWS: upwelling strength (m^3 s^{-1} (100 m)$^{-1}$); EKE: eddy-kinetic energy (cm^2 s^{-2})

[c]: all listed coefficients are statistically significant at the 99% level, i.e., $p < 0.01$.

Table 2: Summary of model setups for the CalCS.

Case	Grid	Topography	Momentum equations	EKE† ($cm^2\ s^{-2}$)	NPP† (mol C $m^{-2}\ yr^{-1}$)
Standard	5 km	5 km	standard	185	10.8
Standard 60 km topo	5 km	as 60 km	standard	162	10.9
Medium Resolution	15 km	15 km	standard	115	14.9
Medium 60 km topo	15 km	as 60 km	standard	127	14.9
Coarse Resolution	60 km	60 km	standard	44	17.1
Non-Eddy	5 km	5 km	w/o non-linear	38	17.8

†: Average values for the central CalCS, i.e., from Point Conception to north of Cape Mendocino and averaged to 500 km offshore distance.

Table 3: Comparison of net primary production in the California Current System (34°N-42°N). Compared are the results from the standard setup of ROMS with the observationally based estimates of Kahru et al. [1].

Offshore Extent	Area (km^2)	ROMS (mol $m^{-2}\ yr^{-1}$)	Kahru (mol $m^{-2}\ yr^{-1}$)	Difference (mol $m^{-2}\ yr^{-1}$)	Rel. difference (%)
0-100 km	96656	23.0	32.9	-9.9	-30%
100-500 km	420602	8.1	10.9	-2.9	-26%
500-1000 km	588201	1.7	4.7	-3.0	-65%
0-1000 km	1105460	6.0	10.1	-4.1	-41%

Figure 1 Maps of satellite-inferred net primary production (gC m^{-2} yr^{-1}) in the 4 major eastern boundary current upwelling systems. (a) California Current System, (b) Canary Current System, (c) Humboldt Current System, and (d) Benguela Current System. The NPP estimates are based on the Vertically Generalized Production Model (VGPM) [4] and represent the long-term mean for the period from 1997-2004. Also shown is the extent of the 500 km swath, across which the data are analyzed.

Figure 2 As Figure S.1 but for Ekman-driven upwelling strength (m^3 s^{-1} (100 m)$^{-1}$), i.e., a mass flux per 100 m of coastline. This upwelling flux was calculated from daily satellite-derived winds (QuikSCAT). Shown is the long-term average over the period 1999-2004, but only for a 500 km swath along the coast.

Figure 3 As Figure S.1 but for eddy-kinetic energy (cm^2 s^{-2}). Eddy-kinetic energy was estimated from the geostrophic velocity anomalies (relative to the nine-year mean) calculated using the mapped sea level anomaly (SLA) data obtained from merged Topex / Poseidon / ERS / Jason-1 / ENVISAT maps. Shown are the long-term means over the period 1995-2003.

Figure 4 Plots of net primary production (left column), upwelling strength (center column), and eddy-kinetic energy (right column), versus latitude for the 4 major eastern boundary current upwelling systems. First row: California Current System; second row: Canary Current System; third row: Humboldt Current System; and forth row: Benguela

Current System. Shown are the 2° binned and shore-to-500 km averages (150-to-500 km averages for EKE) of the data shown in Figures S.1 - S.3.

Figure 5 Comparison of (a-b) annual mean chlorophyll in the surface layer (mg Chl m^{-3}) and (c-d) vertically integrated net primary production (mol C m^{-2} yr^{-1}) between (a) & (c) the standard model and (b) & (d) observational estimates. The chlorophyll observations are based on SeaWiFS, averaged over the period from 1997 to 2004. Net primary production is based on the Vertically Generalized Production Model (VGPM) [4], with the parameters retuned to fit in-situ observations from the CalCOFI program [1]. The model fields are averages over 5 years.

Figure 6 Taylor diagrams (a-b) of model simulated chlorophyll, (c-d) of model simulated net primary production and (e-f) of modeled sea-surface temperature (SST) in comparison to observations. The results for the annual means are shown (a), (c) & (e), while the results for the seasonal components are depicted in (b), (d) & (f). Seasons were defined by aggregating 3 months starting in January. Each panel shows separately the results for the entire model domain (DOMAIN), for the region north of Cape Mendocino (40.5°N), for central California (Point Conception 34.5°N) to Cape Mendocino, and for the Southern California Bight region (south of Point Conception). The root mean square (RMS) misfit between the model and the observational estimates is given by the distance between the model point and the observation point indicated by the filled circle on the abscissa. For

comparison, the results for the 15 + 5 km model setup employed by Gruber et al. [2] are shown using green symbols.

Figure 7 Vertical sections along CalCOFI line 70, showing observations (left column), and modeled properties (right column) for the annual mean. (a) and (b) Observed and modeled temperature (°C); (c) and (d) observed and modeled salinity; and (e) and (f) observed and modeled nitrate concentration (mmol m^{-3}). CalCOFI line 70 extends from Monterey Bay (37°N, 121.8°W) to the open ocean (32°N, 135°W).

Figure 8 Relationship between net primary production or export production and eddy-kinetic energy in the central part of the California Current System. Also shown are results from a Canary Current System setup of ROMS (data from 12°N to 30°N)[8]. Plotted are the results from various model configurations for the two upwelling systems. The same wind stress was applied in all cases. For the California Current System, the standard configuration at 5 km resolution (5 km) and the non-eddying 5 km setup (5 km non-eddy) form end-members along a decreasing trend of NPP with EKE. The results from the Canary Current System fall generally on the same trend for the respective properties, with NPP exhibiting an even stronger decreasing trend at low EKE. Numerical values for the California Current System are tabulated in Table S.2.

Figure 9 (a)-(d) Maps of depth integrated primary production for four different model configurations. (a) 5 km non-eddy, (b) 60 km, (c) 15 km, and (d) standard eddying 5 km

setup. (e)-(g) Maps of differences of these different configurations relative to the standard 5 km setup shown in (d). See Table S.2 for details about these configurations.

Figure 10 Maps of annual mean nitrate distribution and eddy-induced changes. (a)-(c) average nitrate concentration in the upper pycnocline (100 - 300 m) for (a) the non-eddy simulation, (b) eddy simulation, and (c) for the difference (eddy minus non-eddy). (d)-(f) nitrate concentration along the isopycnal surface σ_θ = 26.2 for (d) the non-eddy simulation, (e) eddy simulation, and (f) for the difference (eddy minus non-eddy). Overlain in (f) with contours is the model simulated eddy-kinetic energy (EKE) in cm^2 s^{-2} highlighting the close spatial correspondence of eddy-induced nutrient loss and high EKE.

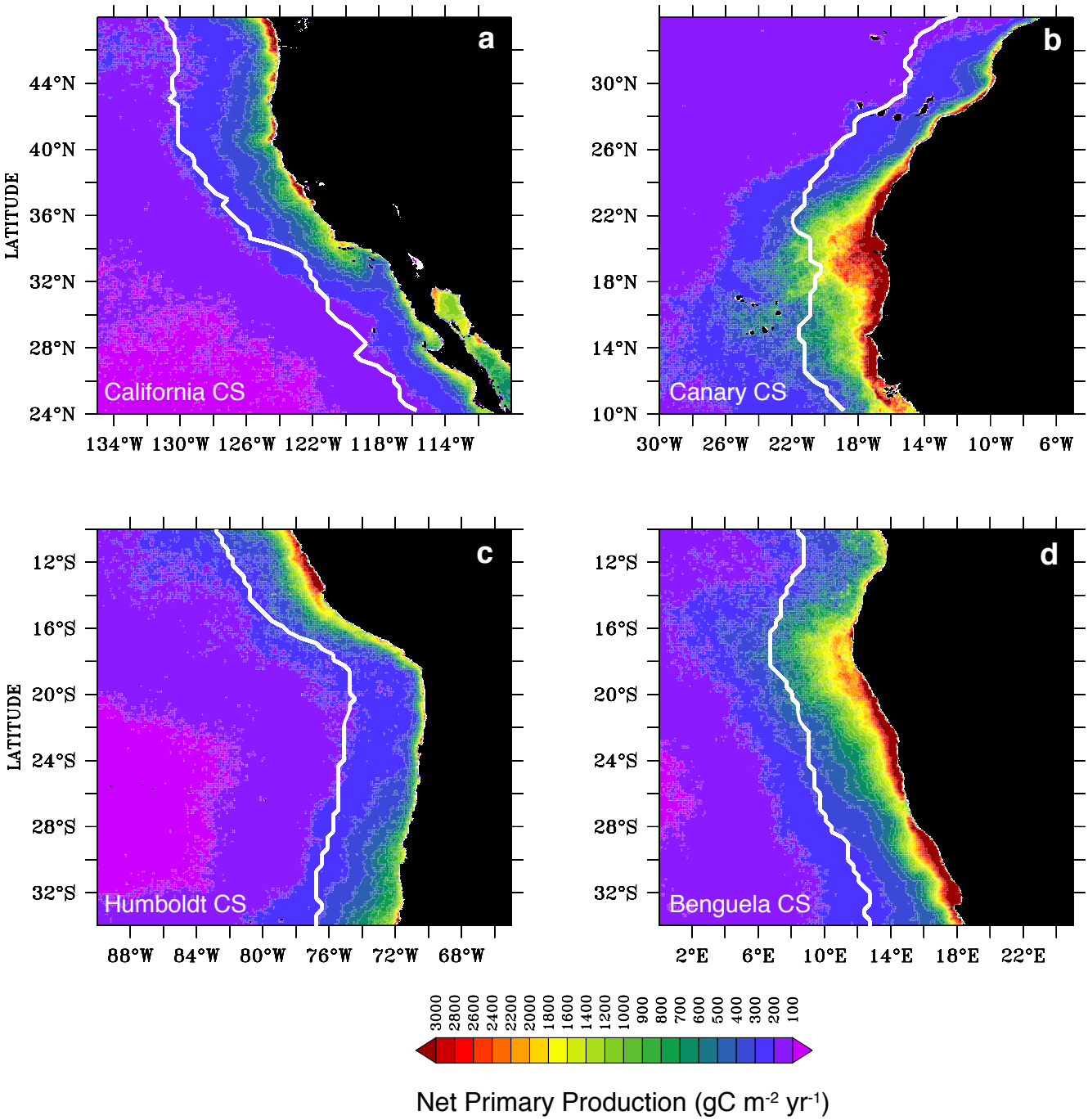

Figure S.1

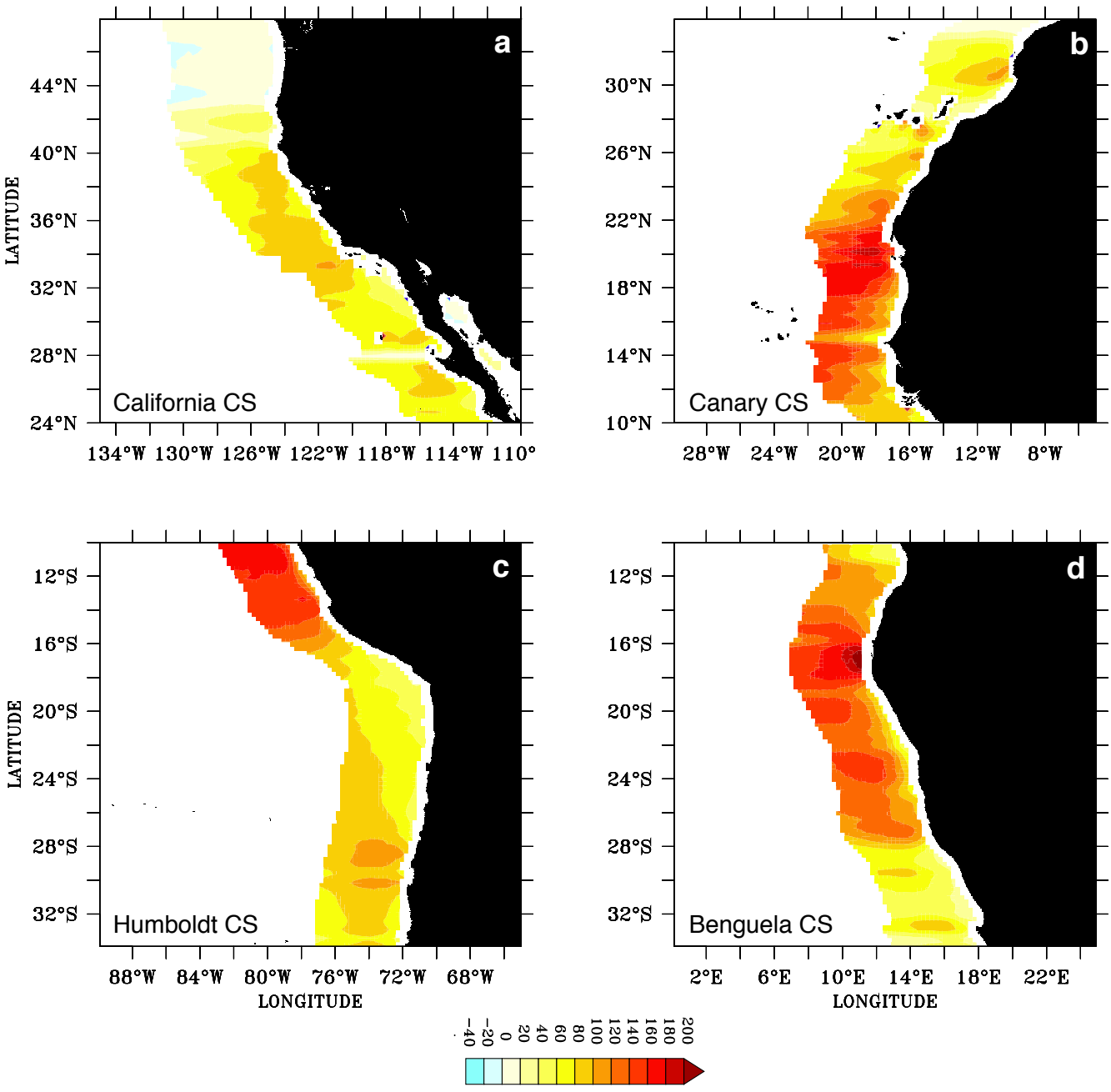

Figure S.2

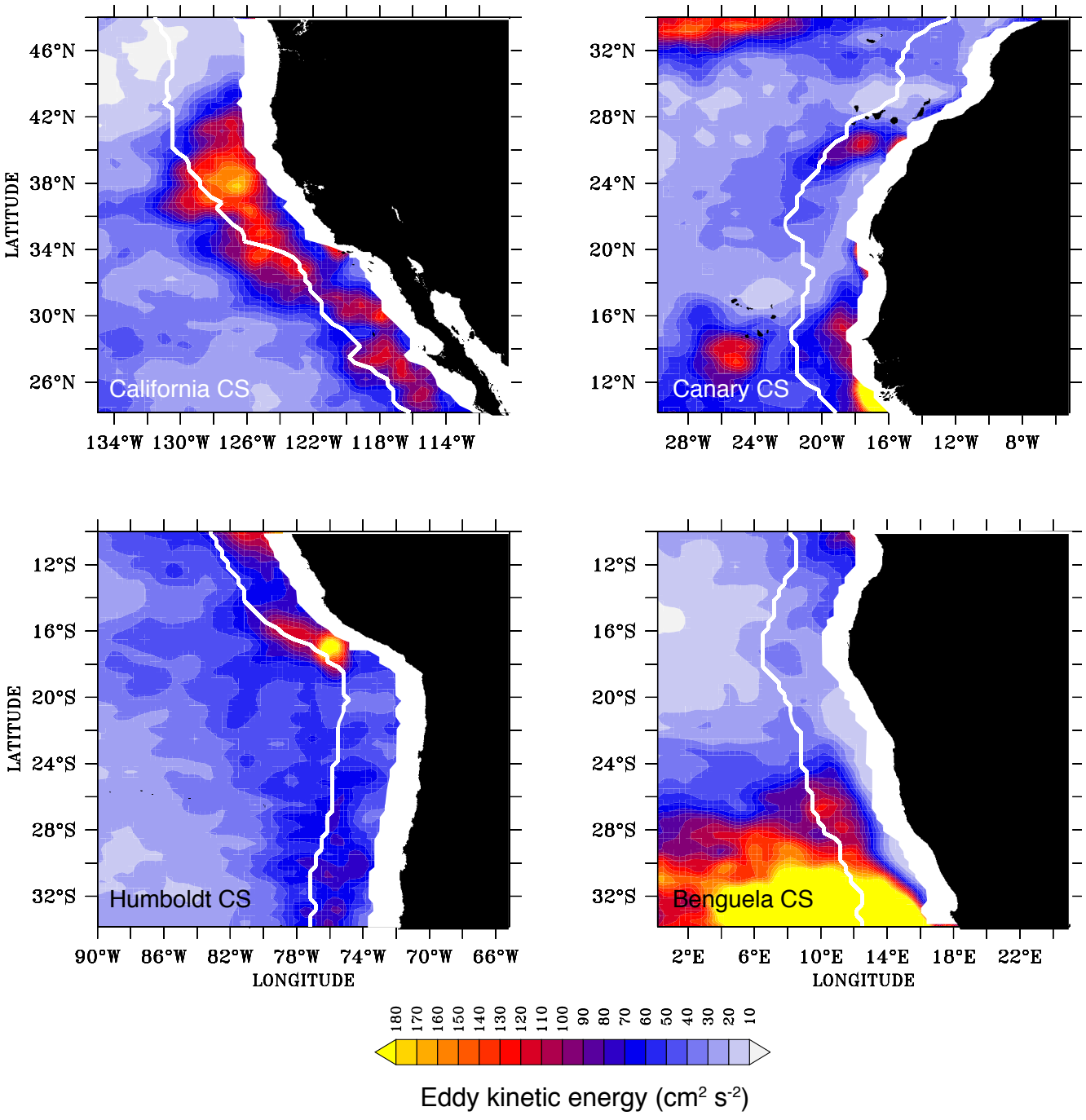

Figure S.3

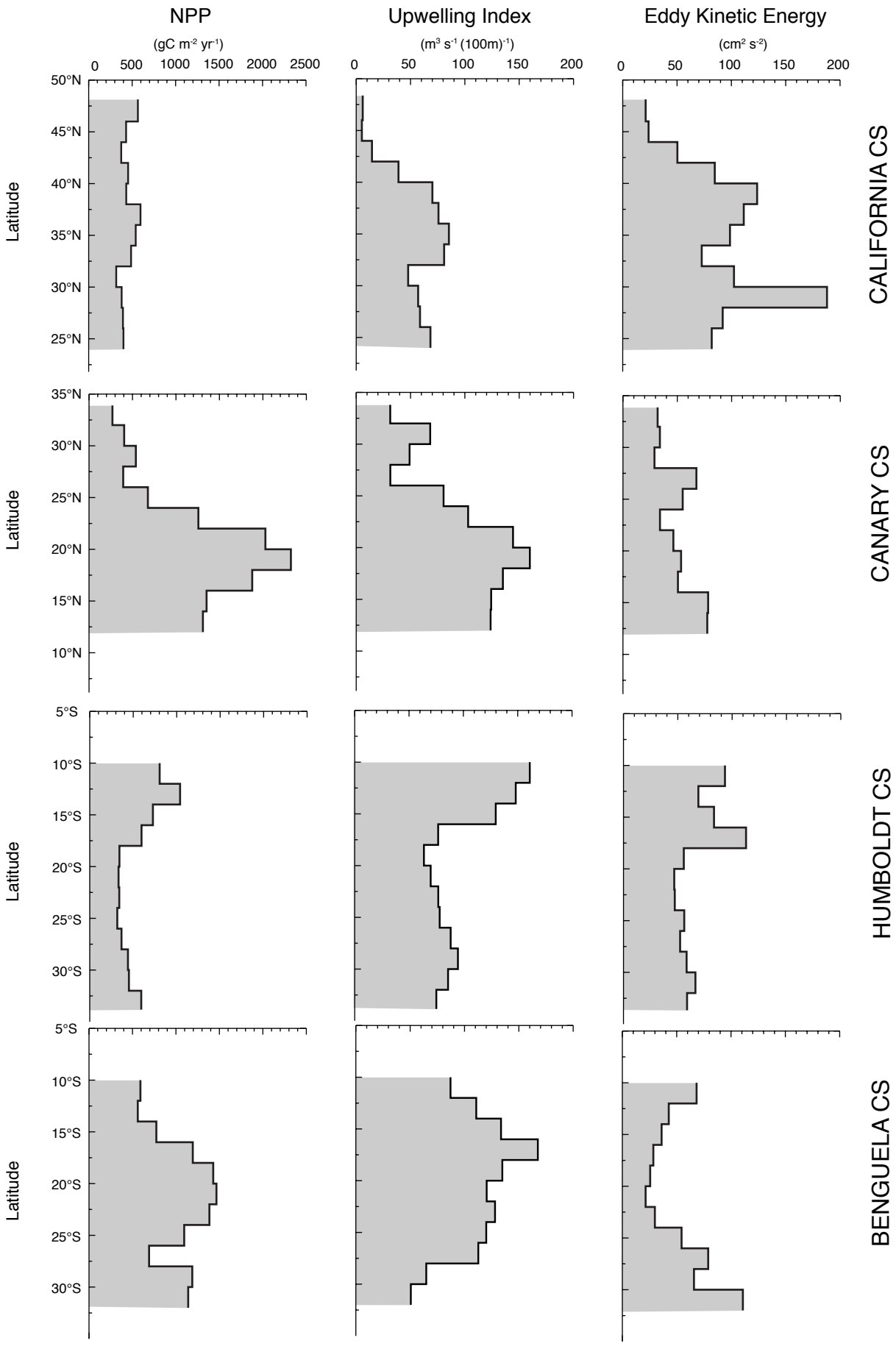

Figure S.4

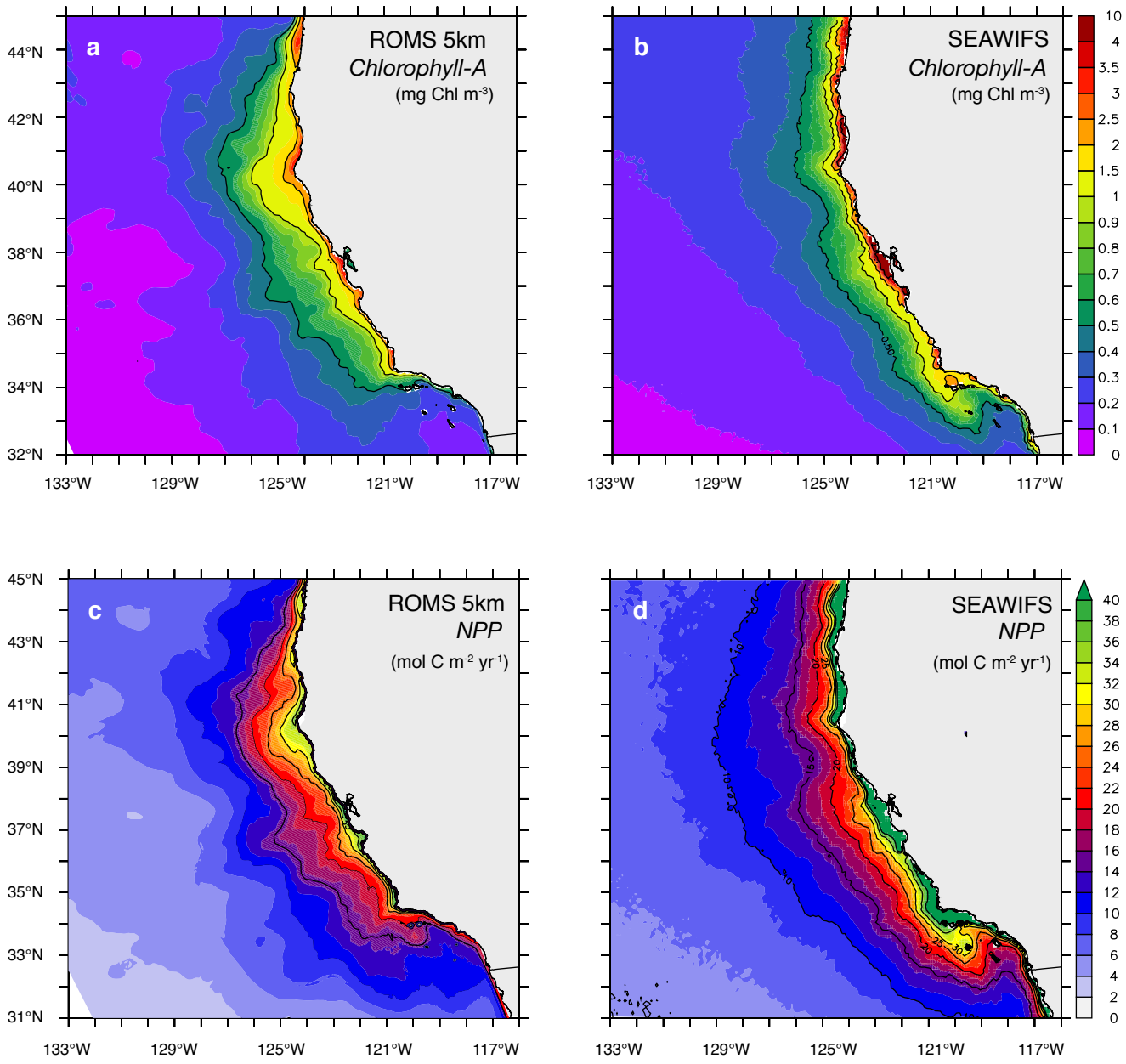

Figure S.5

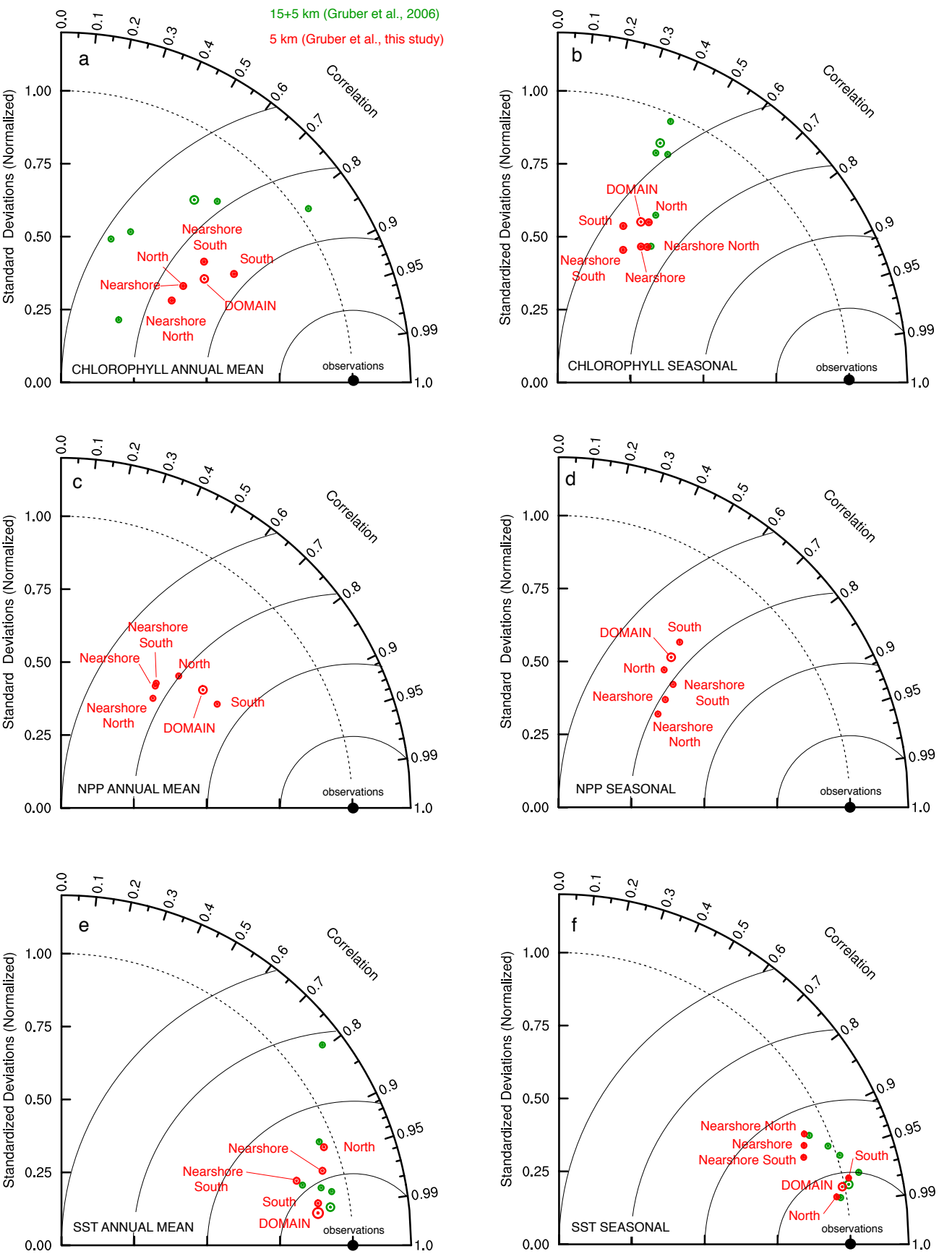

Figure S.6

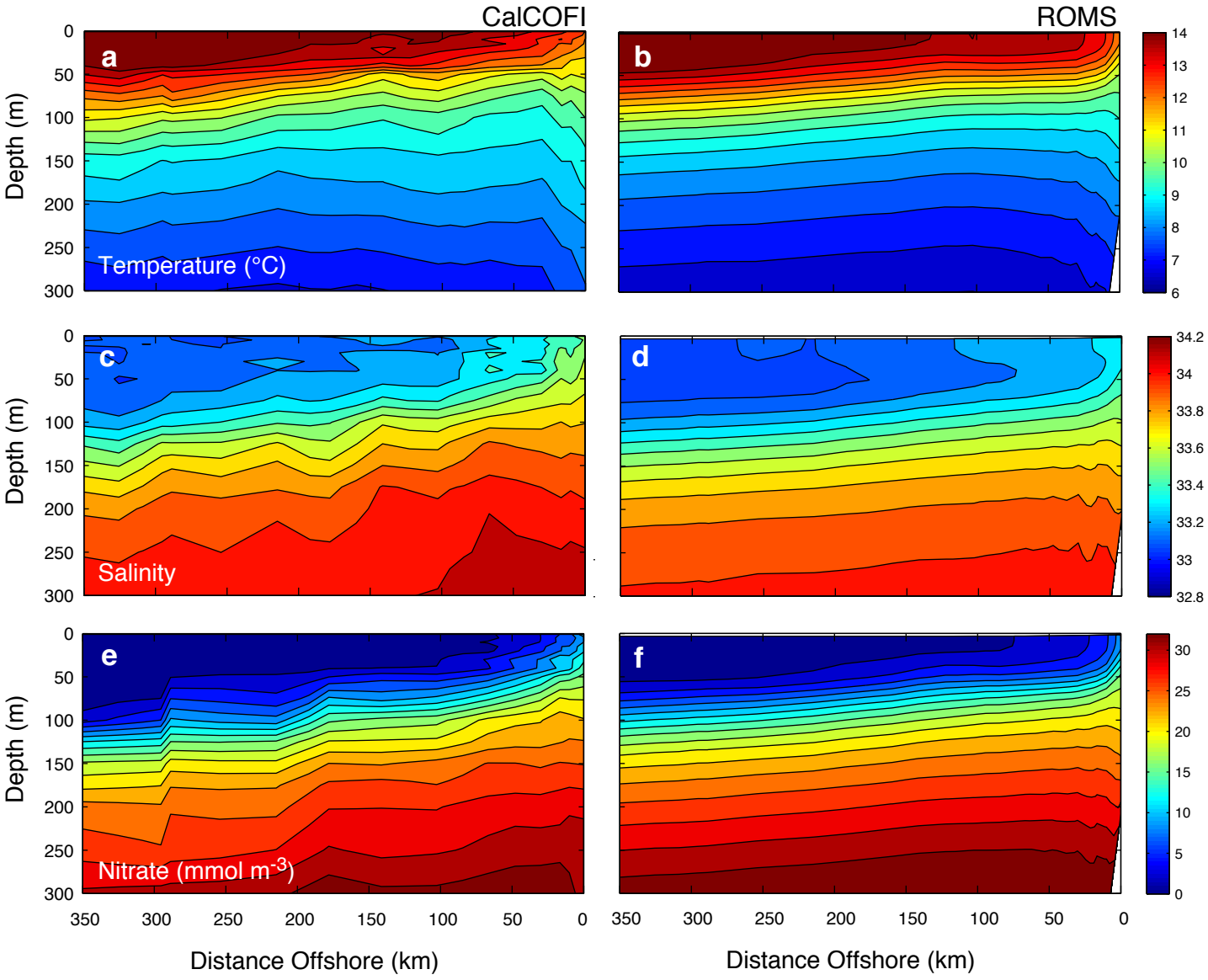

Figure S.7

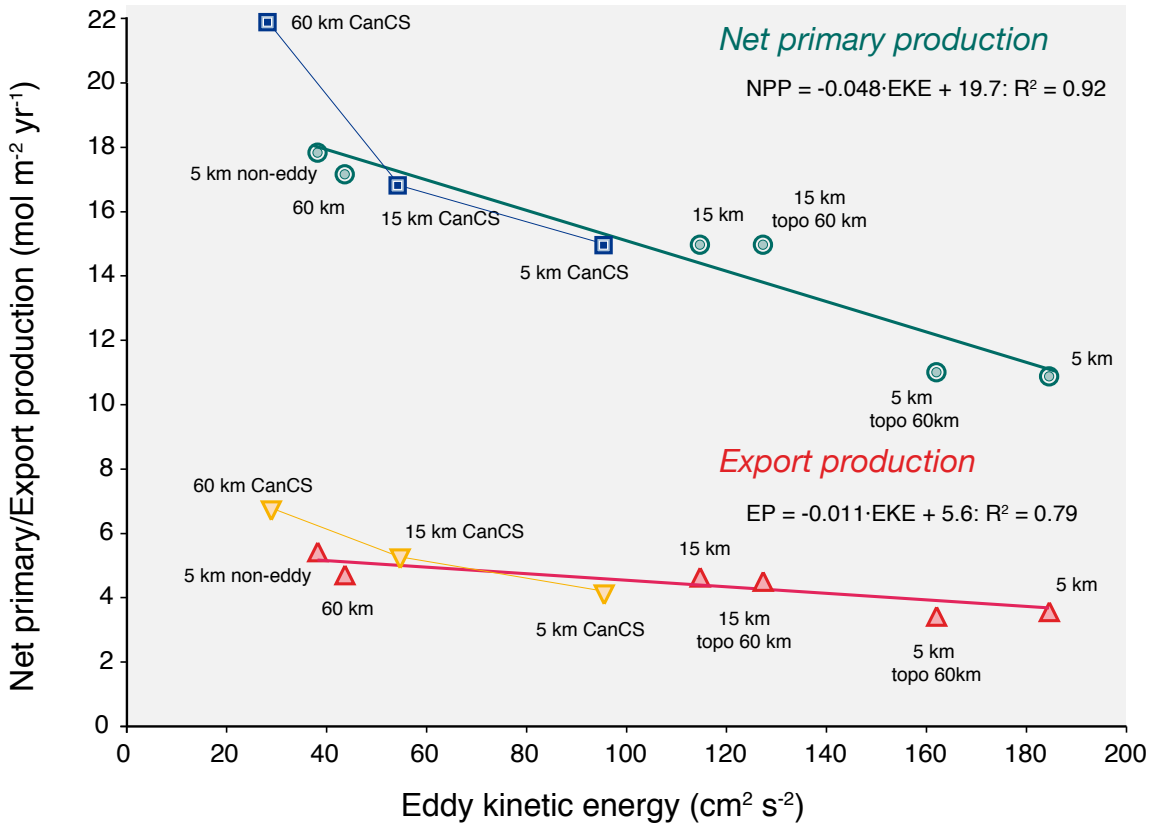

Figure S.8

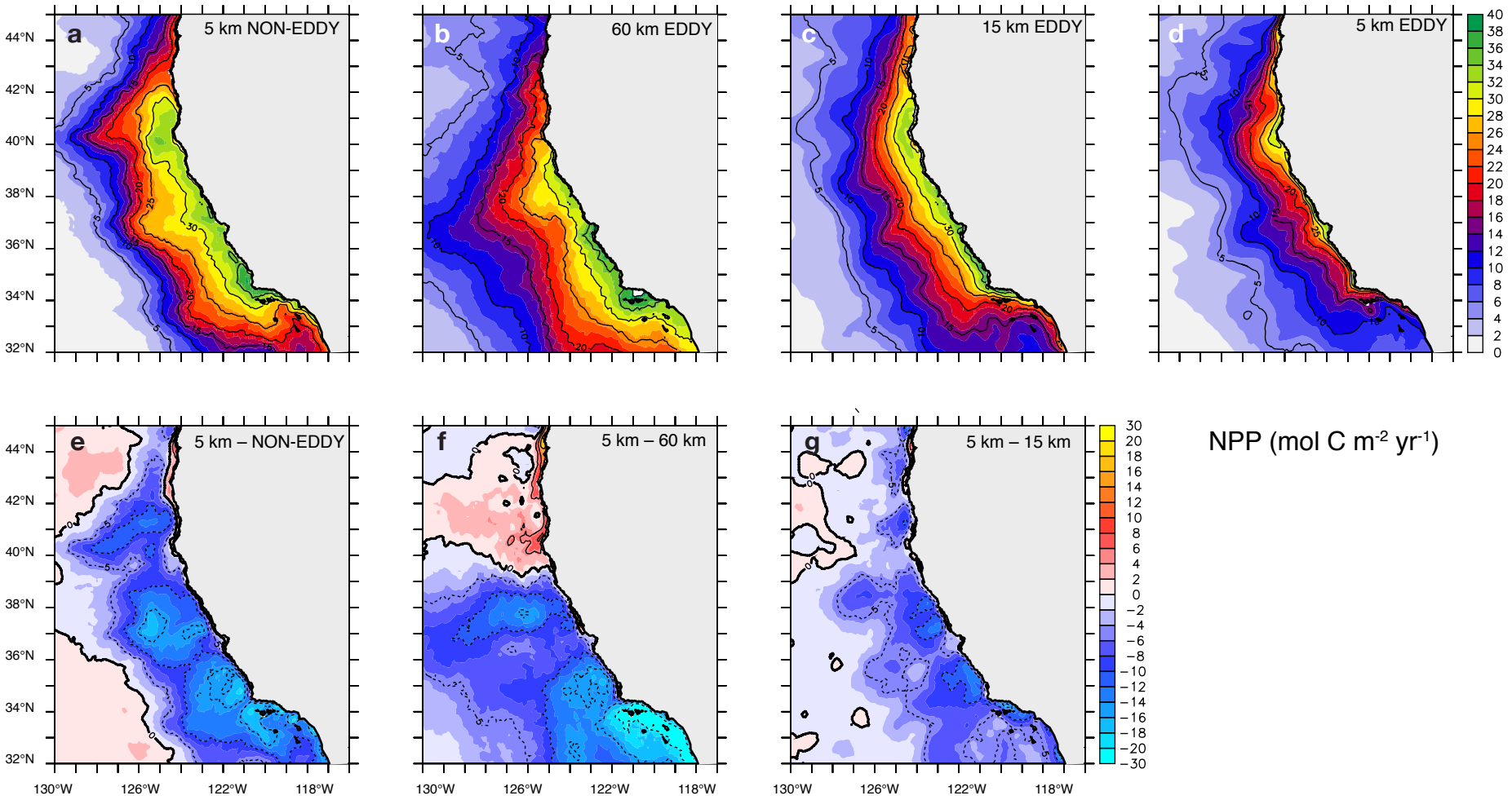

NPP (mol C m^{-2} yr^{-1})

Figure S.9

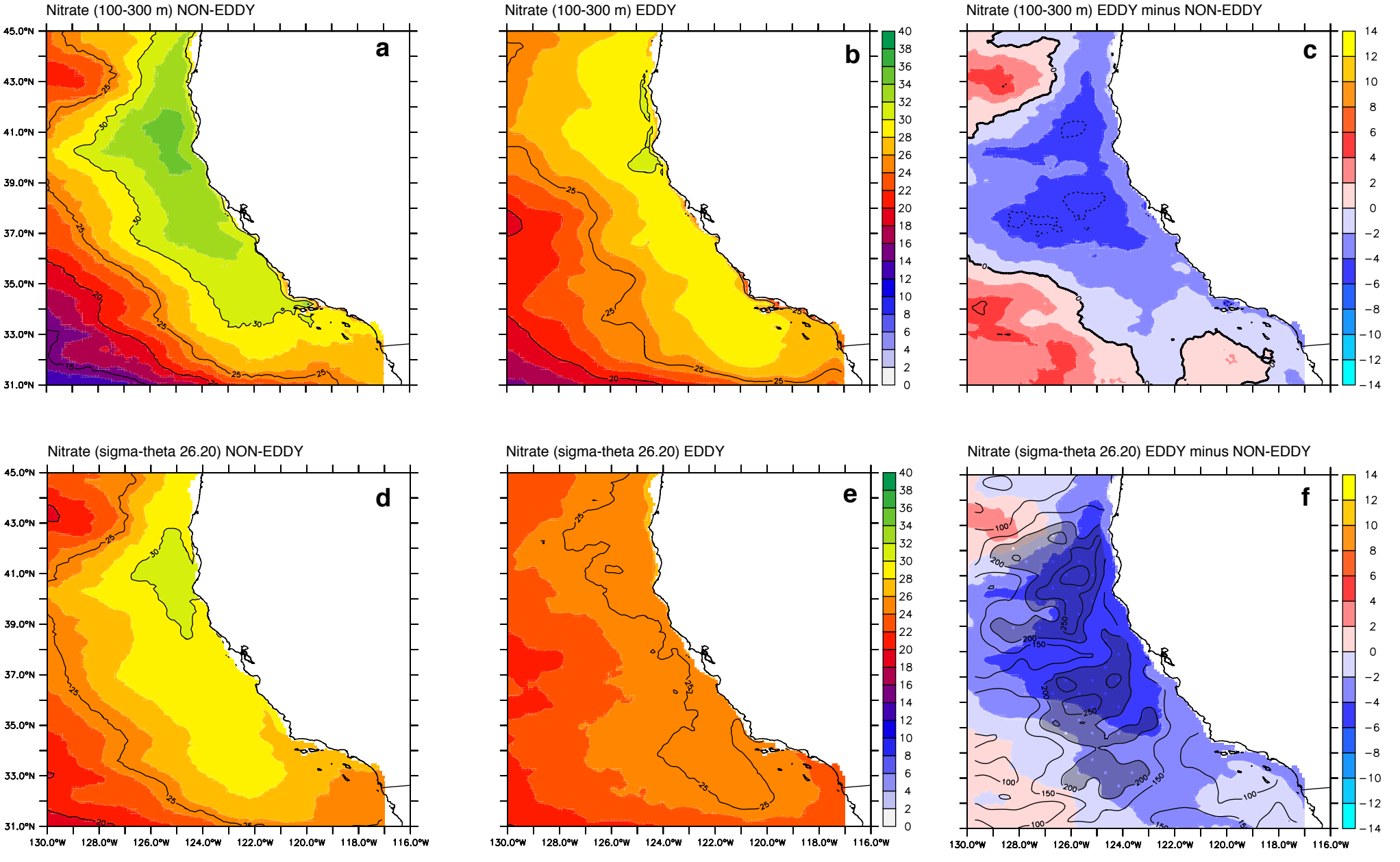

Figure S.10